



Article

# Intergranular Spin Dependent Tunneling Dominated Magnetoresistance in Helimagnetic Manganese Phosphide Thin Films

Baleeswaraiiah Muchharla <sup>1,\*</sup>, Richa Pokharel Madhogaria <sup>1</sup>, Derick Detellem <sup>1</sup>, Chang-Ming Hung <sup>1</sup>, Amit Chanda <sup>1</sup>, Nivarthana W. Y. A. Y. Mudiyansele <sup>1</sup>, Anh Tuan Duong <sup>2,3</sup>, Minh-Tuan Trinh <sup>4</sup>, Sarath Witanachchi <sup>1</sup> and Manh-Huong Phan <sup>1,\*</sup>

<sup>1</sup> Department of Physics, University of South Florida, Tampa, FL 33620, USA; rmadhogaria@usf.edu (R.P.M.); derickd@usf.edu (D.D.); achanda@usf.edu (A.C.); switanach@usf.edu (S.W.)

<sup>2</sup> Faculty of Materials Science and Engineering, Phenikaa University, Hanoi 12116, Vietnam

<sup>3</sup> Phenikaa Research and Technology Institute (PRATI), A&A Green Phoenix Group, 167 Hoang Ngan, Hanoi 13313, Vietnam

<sup>4</sup> Department of Chemistry and Biochemistry, Utah State University, Logan, UT 84322, USA; t.trinh@usu.edu

\* Correspondence: baleeswaraiiahmuchharla@gmail.com (B.M.); phanm@usf.edu (M.-H.P.)

**Abstract:** Helical magnets are emerging as a novel class of materials for spintronics and sensor applications; however, research on their charge- and spin-transport properties in a thin film form is less explored. Herein, we report the temperature and magnetic field-dependent charge transport properties of a highly crystalline MnP nanorod thin film over a wide temperature range ( $2\text{ K} < T < 350\text{ K}$ ). The MnP nanorod films of  $\sim 100\text{ nm}$  thickness were grown on Si substrates at  $500\text{ }^\circ\text{C}$  using molecular beam epitaxy. The temperature-dependent resistivity  $\rho(T)$  data exhibit a metallic behavior ( $d\rho/dT > 0$ ) over the entire measured temperature range. However, large negative magnetoresistance ( $\Delta\rho/\rho$ ) of up to 12% is observed below  $\sim 50\text{ K}$  at which the system enters a stable helical (screw) magnetic state. In this temperature regime, the  $\Delta\rho(H)/\rho(0)$  dependence also shows a magnetic field-manipulated CONE + FAN phase coexistence. The observed magnetoresistance is dominantly governed by the intergranular spin dependent tunneling mechanism. These findings pinpoint a correlation between the transport and magnetism in this helimagnetic system.

**Keywords:** manganese phosphide; helimagnet; magneto-transport



**Citation:** Muchharla, B.; Madhogaria, R.P.; Detellem, D.; Hung, C.-M.; Chanda, A.; Mudiyansele, N.W.Y.A.Y.; Duong, A.T.; Trinh, M.-T.; Witanachchi, S.; Phan, M.-H. Intergranular Spin Dependent Tunneling Dominated

Magnetoresistance in Helimagnetic Manganese Phosphide Thin Films.

*Nanomaterials* **2023**, *13*, 1478. <https://doi.org/10.3390/nano13091478>

Academic Editor: Kai-Huang Chen

Received: 5 April 2023

Revised: 16 April 2023

Accepted: 24 April 2023

Published: 26 April 2023



**Copyright:** © 2023 by the authors. Licensee MDPI, Basel, Switzerland. This article is an open access article distributed under the terms and conditions of the Creative Commons Attribution (CC BY) license (<https://creativecommons.org/licenses/by/4.0/>).

## 1. Introduction

Manganese phosphide (MnP) is a complex magnetic material with multiple exotic magnetic phases. MnP displays various magnetic orderings such as para, ferro, screw, and fan structures, depending on the temperature and applied magnetic field. MnP has an orthorhombic crystal structure with lattice parameters  $a = 5.916\text{ \AA}$ ,  $b = 3.173\text{ \AA}$  and  $c = 5.260\text{ \AA}$ . The unit cell contains four Mn atoms and four P atoms. MnP is a 3d transition metal compound that exhibits a wide range of properties including helimagnetism [1–4], thermoelectricity [5], magneto-calorics [6,7], magneto-optics [8], and superconductivity [9–12]. Single crystal MnP undergoes a paramagnetic (PM) to ferromagnetic (FM) phase transition around room temperature and displays another phase transition from the FM to helical (screw) phase around 50 K in the absence of an external magnetic field [6]. The MnP crystal displays magnetic anisotropy with the  $c$ -axis being the easy direction of magnetization, the  $b$ -axis is the intermediate, and the  $a$ -axis is the hardest one. The phase transition temperatures of the MnP single crystal can be altered by doping with small amounts of Co. With an amount of 0.3 at.% Co doping, both the transition temperatures are lowered by about 5 K, and further increase in the Co concentration to 5% decreases the PM–FM transition to 240 K and suppressing the helimagnetic (HM) transition [13]. In the same study, the topological Hall effect (THE) was observed in the FAN phase of MnP when the magnetic

field was applied along the *b*-axis. Unlike conventional and anomalous Hall effects, THE is typically observed in a phase with the lattice formation of a skyrmion, stabilized by the Dzyaloshinsky–Moriya (DM) interaction, and it appears to occur when conduction electrons acquire the Berry phase while passing through the skyrmion lattice. The THE observed in MnP was reported to decay with 5% doping of Co at the Mn sites [13]. Single crystal MnP, prepared by vapor phase transport, was experimentally investigated to exhibit the de Haas–van Alphen (dHvA) effect [14,15]. The dHvA oscillations were observed with applied fields up to 9.4 T along the *c*-axis at ~1.1 K. The Shubnikov–de Haas-like oscillation was also observed in the high purity single crystal of MnP at 1.5 K in applied fields up to 8 T [16]. Recently, Jiang et al. reported the control of the spin helicity in MnP by using an electric current and a magnetic field, which could be utilized in applications such as magnetic memories based on the spin internal degrees of freedom [17].

While previous studies focused on the transport and spin properties of MnP single crystals [13–18], device applications would be realized mostly on thin films [19]. We have recently reported a comprehensive magnetic study on highly crystalline MnP nanorod films in which the magnetic phase diagrams have been constructed demonstrating the co-existing magnetic phases for the in-plane and out-of-plane field orientations [20]. These findings have motivated us to investigate the charge and spin transport properties of the MnP nanorod film over a wide temperature range ( $2\text{ K} < T < 350\text{ K}$ ) in magnetic fields up to 8 T. In agreement with the previously reported transport results on MnP single crystals [13,17,19,21], a metallic conducting nature is also observed for the MnP nanorod film. However, two distinct temperature regimes have been observed, above and below the FM–HM transition temperature (~50 K), where electrical resistivity ( $\rho$ ) shows a linear temperature dependence for  $T > 50\text{ K}$  and a non-linear power law dependence for  $T < 50\text{ K}$ . Interestingly, we have observed, for the first time, a large negative magnetoresistance ( $\Delta\rho/\rho$ ) of up to 12% and a magnetic-field-manipulated CONE + FAN phase coexistence in this low temperature region ( $T < 50\text{ K}$ ). These findings relate the charge–spin properties characteristic for itinerant helimagnetic systems such as MnP.

## 2. Materials and Methods

MnP nanorod films were grown on Si (100) substrates using molecular beam epitaxy while maintaining the substrate at a temperature of 500 °C. The details of MnP nanorod thin film growth can be found elsewhere [19]. The crystal phase characterization of the MnP thin films was carried out using a Bruker AXS powder X-ray diffractometer (XRD) (Bruker, Madison, WI, USA) with Cu–K $\alpha$  radiation at room temperature. Field emission scanning electron microscopy (FE-SEM)(JEOL, Tokyo, Japan) was performed to observe microstructural variation in the films grown at different temperatures. Temperature dependent transport measurements were carried out using a four-probe measurement system consisting of a Keithley 2400 source meter and a Keithley 2182a nanovoltmeter (Keithley Instruments, Cleveland, Ohio, USA) integrated with the Physical Property Measurement System (PPMS) from Quantum Design, San Diego, CA, USA. Temperature- and magnetic-field-dependent electrical resistivity and current–voltage ( $I$ – $V$ ) characteristic curves were measured within the wide range of temperature ( $2\text{ K} < T < 350\text{ K}$ ) and applied magnetic field ( $0\text{ T} < \mu_0 H < 8\text{ T}$ ).

## 3. Results

The XRD pattern of the MnP thin film sample displays the orthorhombic MnP peaks as defined in Figure 1a (ICDD-JCP2, No. 03-065-2597). The energy dispersive X-ray spectroscopy (EDS) spectrum of the MnP film, as shown in an inset of Figure 1a, consistently confirms the presence of Mn and P elements in the MnP film grown on the Si substrate. Surface morphology of the MnP film was characterized by FE-SEM, as presented in Figure 1b, indicating closely packed MnP nanorods grown vertically out of the plane on the Si substrate. The inset of Figure 1b displays an AFM image of the MnP film. A typical four-probe method was utilized as depicted in the schematic (Figure 2a) to acquire the transport data

of the MnP film device. To understand the transport nature of the MnP film, we measured the temperature dependent resistivity over a wide range ( $10\text{ K} < T < 305\text{ K}$ ) and the result is displayed in Figure 2b. The room temperature resistivity is of  $4.25 \times 10^{-4}\ \Omega\text{ cm}$ , and the value decreases with lowering temperature (Figure 2b) indeed shows a metallic behavior for this film in the entirely measured temperature range. This type of metallic nature is in agreement with previous reports on MnP [13,17,19,21]. In the absence of an external magnetic field, bulk MnP undergoes a PM–FM phase transition at  $\sim 290\text{ K}$  and then stabilizes into a stable helical (screw) phase below  $\sim 50\text{ K}$ . The observed  $\rho(T)$  behavior of the MnP film indicates that two slope changes right around these magnetic transitions exist, indicating a correlation between the conductivity and magnetism in this system. These phase transitions are clearly evidenced with the slope changes on the derivative of resistivity versus temperature plot displayed (blue circles) on the right  $y$ -axis of Figure 2b. Temperature-dependent magnetization ( $M$ – $T$ ) behavior is displayed in Figure 2d under a field-cooled warming protocol for  $2\text{ K} < T < 370\text{ K}$ . A PM–FM phase transition is clearly observed around  $300\text{ K}$ , followed by the FM transition to the stable helical (screw) state transition at  $\sim 50\text{ K}$  as shown in Figure 2d. Note that the onset temperature of the FM to HM transition occurs at  $\sim 100\text{ K}$  and stabilizes to the helical phase below  $50\text{ K}$ . The derivative of zero-field-cooled magnetization with respect to temperature plotted (blue circles) on the right  $y$ -axis of Figure 2d represents the PM–FM phase transition around  $300\text{ K}$ , with the FM to HM onset at  $\sim 100\text{ K}$  and stabilized to the HM phase below  $50\text{ K}$ . Previous studies have shown similar magnetic phase transitions in helimagnetic MnP samples. For instance, 2D MnP single crystals grown using a conventional vapor deposition (CVD) technique exhibited a paramagnetic–ferromagnetic transition at  $303\text{ K}$  and the helical magnetic (screw) state at  $38\text{ K}$  [22]. Whereas Andrés et al. reported a large variation in the ferromagnetic–screw transition temperature for bulk MnP ( $\sim 47\text{ K}$ ), the MnP thin film ( $\sim 67\text{ K}$ ), and the MnP nanocrystals ( $\sim 82\text{ K}$ ) embedded in the GaP epilayers [23]. Note that the phase transition temperatures varied, depending on the size and shape of the nanocrystals present in the samples. In the present study, it is the formation of MnP nanorods that led to the occurrence of the onset of the screw phase transition at  $\sim 100\text{ K}$ .

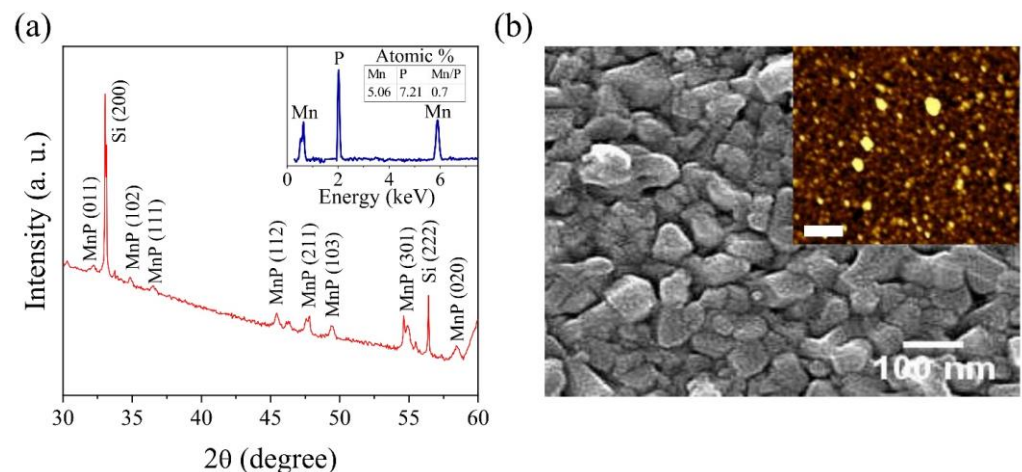


**Figure 1.** Structural and morphological characterization of the MnP film: (a) XRD pattern of the MnP sample. The inset displays EDS spectra of the MnP film.; (b) SEM image of closely packed MnP nanorods grown vertically on the Si substrate. The inset displays an AFM image of the MnP film. The scale bar on the AFM image is  $500\text{ nm}$ .

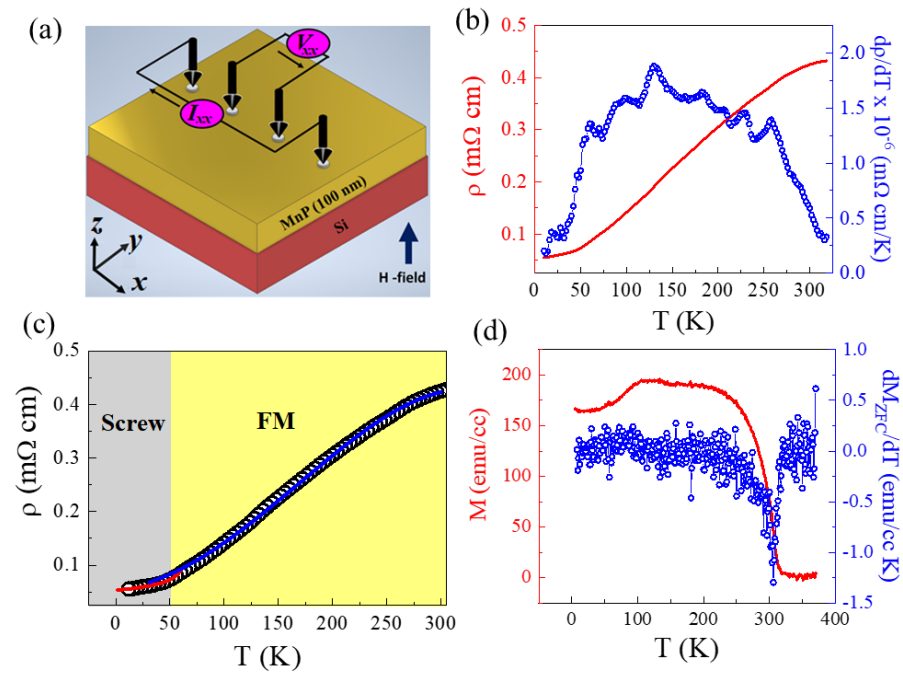


**Figure 2.** Temperature-dependent electrical transport properties of the MnP film: (a) Typical device schematic indicating the device structure with four-probe configuration; (b) temperature dependence of the electrical resistivity in the temperature range  $10 \text{ K} < T < 305 \text{ K}$ . The plot on the right  $y$ -axis (blue circles) displays the derivative of resistivity versus temperature; (c) temperature dependence of the electrical resistivity plot indicating the screw and FM temperature regions; (d) temperature dependence of magnetization,  $M$  vs.  $T$  curves, under a zero field-cooled–warming protocol. The plot on the right  $y$ -axis (blue circles) displays the derivative of zero field cooled magnetization with respect to temperature.

In this study, the temperature dependence of electrical resistivity is broken down into two distinct temperature regimes, separated at  $\sim 50 \text{ K}$ , below which the system enters a stable helical (screw) magnetic state. For  $T > \sim 50 \text{ K}$ , a monotonic decrease in electrical resistivity is seen with decrease in temperature. For  $T < 50 \text{ K}$ , however, a non-linear temperature dependence of electrical resistivity with decrease in the temperature is observed. Electrical resistivity of a metallic ferromagnet [24] can be explicitly described as

$$\rho(T) = \rho_0 + \rho_{e-e} + \rho_{e-ph} + \rho_{e-mag}, \quad (1)$$

where  $\rho_0$  is a temperature independent term which corresponds to the contribution from impurity scattering,  $\rho_{e-e}$  accounts for the Coulombic interaction between the conduction electrons ( $T^2$  dependence) [25],  $\rho_{e-ph}$  is associated with the electron–phonon interaction, and  $\rho_{e-mag}$  accounts for electron–magnon interactions. In case of two-magnon scattering mechanism,  $\rho_{e-mag}$  varies as  $\sim T^{4.5}$  at low temperatures and  $\sim T^{3.5}$  in the high temperature region [26]. It should be recalled that bulk MnP is a helimagnet, which exhibits complex magnetic phases with respect to temperature and magnetic field. In the absence of an external magnetic field, bulk MnP undergoes a PM–FM phase transition at  $\sim 290 \text{ K}$  and then stabilizes into a helical (screw) phase below  $\sim 50 \text{ K}$  [20]. It is clear from Figure 2c that  $\rho(T)$  for our MnP film undergoes two consecutive slope changes: one around the PM–FM phase transition ( $\sim 290 \text{ K}$ ) and another around  $\sim 50 \text{ K}$  that coincides with the FM to screw phase transformation. Therefore, the electrical transport mechanism in our MnP film is strongly correlated to the nature of the magnetic ground state. Distinct magnon dispersion is expected above and below  $50 \text{ K}$ , which also indicates the different nature of the electron–magnon scattering mechanisms in these two different temperature regimes. It is known that the contribution from the scattering of electrons by lattice phonons follows

$T^5$ -behavior [27] in the low temperature region but shows a  $T$ -linear dependence in the high temperature region [28]. Considering the  $T$ -linear behavior of the electron–phonon interaction in the high temperature region, we fitted the  $\rho(T)$  curve for  $50 \text{ K} < T \leq 300 \text{ K}$  (solid red line) with the following expression:

$$\rho(T) = \rho_0 + \rho_{e-ph} + \rho_{e-e} + \rho_{e-mag} = \rho_0 + \rho_1 T + \rho_2 T^2 + \rho_{3.5} T^{3.5} \quad (2)$$

From the fit, we obtained  $\rho_0 = 5.4 \times 10^{-5} \Omega \text{ cm}$ ,  $\rho_1 = 2.27 \times 10^{-7} \Omega \text{ cm}\cdot\text{K}^{-1}$ ,  $\rho_2 = 7.25 \times 10^{-9} \Omega \text{ cm}\cdot\text{K}^{-2}$ , and  $\rho_{3.5} = -7.52 \times 10^{-13} \Omega \text{ cm}\cdot\text{K}^{-3.5}$ . Considering the  $T^5$ -behavior of the electron–phonon interaction in the low temperature region, we fitted the  $\rho(T)$  curve in the temperature regime  $10 \text{ K} \leq T \leq 50 \text{ K}$  (black line) with the following expression,

$$\rho(T) = \rho_0 + \rho_{e-ph} + \rho_{e-e} + \rho_{e-mag} = \rho_0 + \rho_5 T^5 + \rho_2 T^2 + \rho_{4.5} T^{4.5} \quad (3)$$

The values of  $\rho_0$ ,  $\rho_5$ ,  $\rho_2$ , and  $\rho_{4.5}$  obtained from the fit are  $5.41 \times 10^{-5} \Omega \text{ cm}$ ,  $2.45 \times 10^{-13} \Omega \text{ cm}\cdot\text{K}^{-5}$ ,  $1.12 \times 10^{-8} \Omega \text{ cm}\cdot\text{K}^{-2}$ , and  $-1.93 \times 10^{-12} \Omega \text{ cm}\cdot\text{K}^{-4.5}$ , respectively. It is evident that the electron–electron scattering is the dominating mechanism, as compared to the electron–magnon scattering, governing the electrical transport in the MnP film. Furthermore, it is clear from the fitting parameters that the strength of the electron–electron inelastic scattering becomes stronger at low temperatures. It should be recalled that bulk MnP is a helimagnet, which exhibits complex magnetic phases with respect to the temperature and magnetic field [17]. Transport studies on needle-shaped MnP single crystals grown using the Sn-flux method by Cheng et al. also showed a  $T^2$  dependence of electrical resistivity at low temperatures and interestingly a superconducting behavior upon the application of a high pressure ( $\sim 8 \text{ GPa}$ ) at  $\sim 1 \text{ K}$ , the MnP system was driven into the superconducting state [11].

Magneto-transport measurements were carried out on the same sample by applying a magnetic field perpendicular to the plane of the film. Temperature dependence of electrical resistivity,  $\rho(T)$ , was studied in the temperature range  $10 \text{ K} \leq T \leq 305 \text{ K}$  at different magnetic field strengths as shown in the main panel of Figure 3a. The trend of  $\rho(T)$  in presence of the external magnetic field is similar to that observed in a zero magnetic field. However, the value of  $\rho$  drops significantly with increasing magnetic field strength at low temperatures, especially below  $\sim 50 \text{ K}$  ( $\rho$  drops from  $0.05 \text{ m}\Omega \text{ cm}$  for  $\mu_0 H = 0 \text{ T}$  to  $0.04 \text{ m}\Omega \text{ cm}$  for  $\mu_0 H = 5 \text{ T}$  at  $T = 10 \text{ K}$ ), indicating that the electrical transport is strongly correlated to the HM state at low temperatures. A decrease in electrical resistivity with the application of magnetic field resulted in a negative magnetoresistance. The temperature dependence of magnetoresistance was estimated using the percentage change as,

$$\text{MR}(\%) = \{[\rho(T, \mu_0 H) - \rho(T, \mu_0 H = 0 \text{ T})] / \rho(T, \mu_0 H = 0 \text{ T})\} \times 100 \quad (4)$$

The inset of Figure 3a shows the temperature dependence of magnetoresistance at  $\mu_0 H = 5 \text{ T}$ , which clearly shows a drastic enhancement of negative magnetoresistance below  $50 \text{ K}$ . To verify this enhancement of magnetoresistance, additional experiments were performed to determine the magnetic field dependence of magnetoresistance at different temperatures between  $2$  and  $300 \text{ K}$  by sweeping magnetic field between  $-7$  and  $+7 \text{ T}$ , as shown in Figure 3b. The magnetic field dependence of magnetoresistance is estimated using the relative resistivity ratio:  $\text{MR}(\%) = \{[\rho(H) - \rho(H = 0)] / \rho(H = 0)\} \times 100$ . It is evident that the value of negative magnetoresistance is dramatically enhanced below  $50 \text{ K}$ , which underscores a strong correlation between the transport mechanism and the magnetic phase transition from the FM to the screw phase. The value of  $\text{MR}(\%)$  reaches the highest value of  $12.5\%$  at  $2 \text{ K}$ , which is nearly consistent with the temperature-dependent magnetoresistance data presented in the inset of Figure 3a. A dominant butterfly shape of magnetoresistance isotherms with considerable hysteresis appears to occur at low temperatures below  $50 \text{ K}$ . The inset of Figure 3b displays magnetoresistance versus magnetic field at  $2 \text{ K}$  with magnetic

field sweep directions indicated by red and blue arrows. The hysteresis becomes strongly suppressed for  $50\text{ K} < T < 100\text{ K}$  and diminished for  $T > \sim 100\text{ K}$  at which the onset temperature of the FM to HM transition is observed.

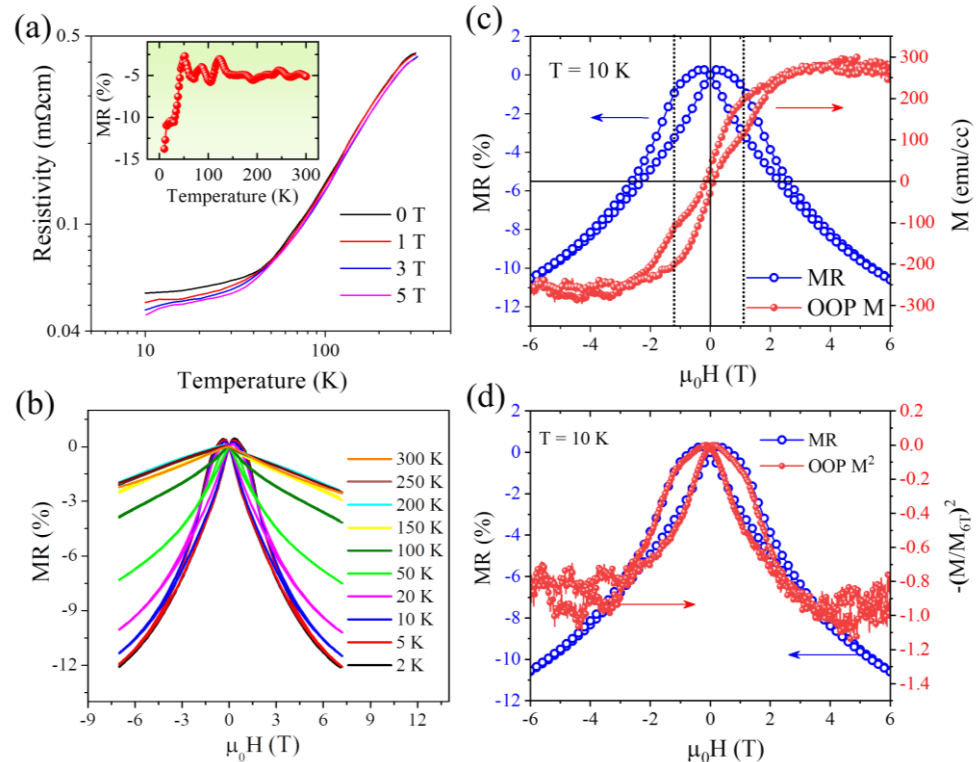


**Figure 3.** Temperature and magnetic field dependent magneto-transport properties of the MnP film; (a) Temperature dependence of the resistivity in the temperature range  $10\text{ K} < T < 305\text{ K}$  in the presence of discrete magnetic fields. The inset shows the temperature dependence of magnetoresistance at  $\mu_0 H = 5\text{ T}$ ; (b) magnetoresistance versus magnetic field at various temperatures. The inset displays magnetoresistance versus magnetic field at  $2\text{ K}$ . Red and blue arrows indicate the direction of magnetic field sweep; (c) comparison of magnetoresistance (left-y-scale) and out-of-plane (OOP) magnetization (right-y-scale) at  $T = 10\text{ K}$ ; and (d) correlation between magnetoresistance (left-y-scale) and reduced squared magnetization (right-y-scale) at  $T = 10\text{ K}$  signifying a dominant role of intergranular tunneling.

The nature of the magnetic field dependence of magnetoresistance for our MnP nanorod thin films has certain similarities to spin-dependent tunneling magnetoresistance observed in ferromagnetic nanoclusters embedded in a nonmagnetic insulating/semiconducting matrix, e.g., Co–SiO<sub>2</sub> granular films [29], ferromagnetic cobaltite La<sub>0.85</sub>Sr<sub>0.15</sub>CoO<sub>3</sub> [30], etc. The probability of tunneling of conduction electrons depends on the relative orientation of the magnetic moments of neighboring grains, which increases when these magnetic moments are aligned parallel to each other. Such a conducting mechanism is quite plausible in our MnP system because of several interfaces formed along the aligned nanorods. In the absence of an external magnetic field, the magnetic moments of the adjacent grains are randomly oriented, thus limiting conduction electrons to tunneling between these grains. As the applied magnetic field increases, these magnetic moments will be aligned with the field direction, giving rise to the enhanced intergranular tunneling of conduction electrons and hence the lower resistance state. In case of inelastic tunneling of electrons across a single potential barrier, the tunneling magnetoresistance can be expressed as [31]

$$\frac{\Delta\rho}{\rho} = -\frac{P^2 m^2}{1 + P^2 m^2} \quad (5)$$

where  $P$  is the degree of spin polarization and  $m$  is the reduced magnetization. For a granular film, it has been theoretically shown that  $\frac{\Delta\rho}{\rho} \propto m^2$  [29]; which simply indicates that the field dependence of magnetoresistance should follow the trend of squared magnetization. In Figure 3c, we plotted the magnetoresistance isotherm at  $T = 10$  K together with the  $M(H)$  hysteresis loop measured in the out-of-plane (OOP) configuration at the same temperature. It is evident that the peak in magnetoresistance occurs around the coercive field, which is followed by a slope change in magnetoresistance that coincides with the high field switching behavior in the OOP  $M(H)$ . As shown in Figure 3d, the magnetoresistance isotherm exactly follows the field dependence of reduced squared magnetization  $(M/M_{6T})^2$  at  $T = 10$  K, which indicates that the observed magnetoresistance in our MnP nanorod thin film is dominated by the intergranular spin-dependent tunneling mechanism.

To affirm the negative MR effect and gain further insight into the correlation between the transport and magnetism in the MnP film,  $I$ - $V$  characteristic curves were also measured by varying temperature (10–300 K) and magnetic field (0–8 T). All  $I$ - $V$  curves measured for the MnP sample display linear behavior indicating the ohmic nature of the sample. As can be observed in Figure 4a, in the absence of an applied magnetic field, the slopes of the  $I$ - $V$  curves increase with decrease in the temperature, indicating the increase/decrease in conductivity/resistivity with lowering temperature, which is in full agreement with that shown in Figure 2a. A similar behavior of the  $I$ - $V$  curves taken at different temperatures is observed in the presence of 8 T, as shown Figure 4b. Figure 4c,d displays the  $I$ - $V$  curves at constant temperatures (Figure 4c at 300 K and Figure 4d at 10 K) with magnetic field varying from 0 to 8 T. While at room temperature, the slopes of the  $I$ - $V$  curves slightly increased with the applied magnetic field since MnP is in the PM region. On the other hand, the change at 10 K is more pronounced with the applied magnetic field, as shown in Figure 4c,d. This results in the sizable MR effect, which is in full agreement with that shown in Figure 3c.

In order to establish this correlation, resistivity values obtained from the slopes of the  $I$ - $V$  characteristics were first plotted against temperature (2–200 K) and magnetic field (0–8 T) in a 2D-surface plot as shown in Figure 5a. As expected, the electrical resistivity decreases with decreasing temperature and increasing magnetic field. Figure 5c displays the magnetoresistance data for the same ranges of temperature and magnetic field as in Figure 5a. An increase in negative magnetoresistance is also observed with decrease in the temperature and increase in the magnetic field. The increment can be observed from the transition from the HM to FM + HM region. Figure 5b,d displays the 2D-surface plots of the resistivity and magnetoresistance data in the temperature range (200–350 K) and in the magnetic field range (0–8 T). A stable FM phase is observed from  $\sim 230$  down to  $\sim 100$  K which is the onset temperature of the FM–HM transition. Below 100 K, a mixed phase (FM + HM) coexists, and the HM phase is dominant below  $\sim 50$  K. Very interesting features are observed below 50 K from the magnetoresistance data as shown in Figure 5c. A constant negative magnetoresistance of about 2% was observed at these temperatures when the applied magnetic field was less than 1.5 T. Further increase in the applied magnetic field ( $1.5 \text{ T} < \mu_0 H < 8 \text{ T}$ ) predominantly increases the negative magnetoresistance (reaching  $\sim 12\%$  at 2 K and 8 T). A distinguishable change in the magnetoresistance behavior at  $\sim 50$  K is related to the transition from the FM to the (complete) screw phase. At a given temperature (e.g., 2 K), the MnP film displayed an obvious change in the MR ratio at the critical fields at which the sample undergoes different magnetic transitions (e.g., CONE, FAN). Interestingly, at  $\sim 300$  K, a negative to positive magnetoresistance is observed for the MnP sample, which is associated with the PM to FM phase transition that occurs at the same temperature. These findings point to a new possibility of controlling the charge transport in HM systems by controlling an external magnetic field. From a fundamental research perspective, our charge–spin–transport study also suggests it as a useful probe of the competing phases' coexistence and the magnetic field-driven conversion of these phases in HM systems such as MnP, adding complementary information to the complex magnetic phase diagrams of these systems.

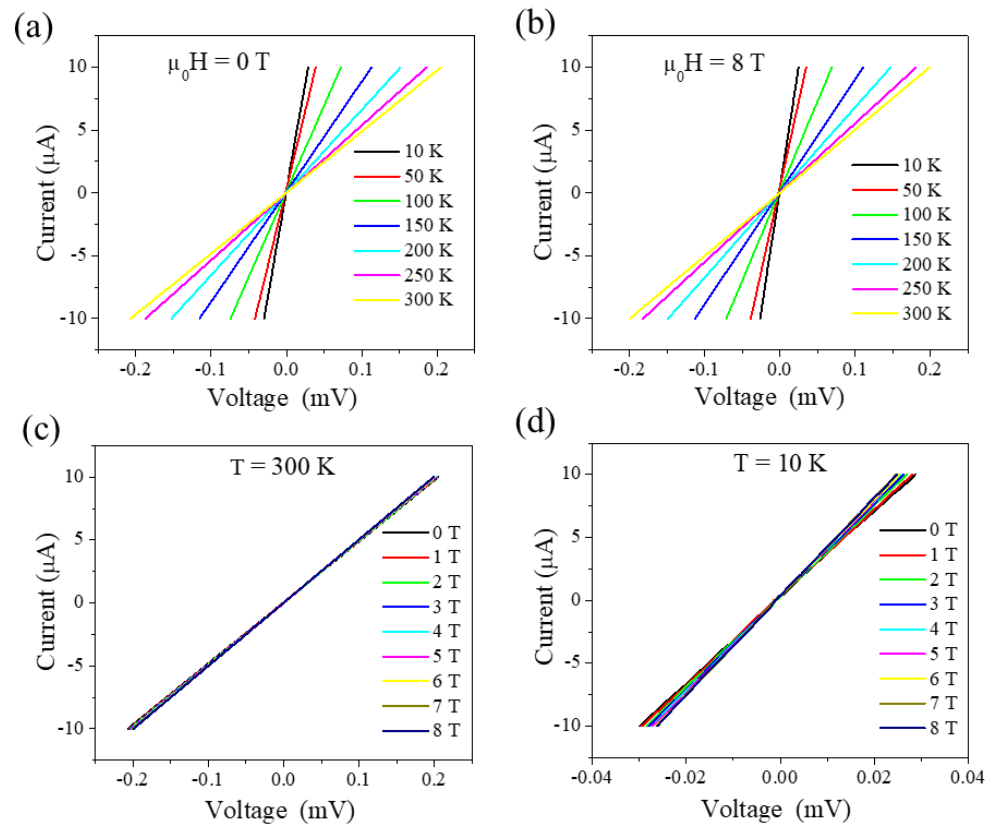


**Figure 4.** *I*-*V* characteristics of the MnP film: at (a)  $\mu_0H = 0$  T and (b)  $\mu_0H = 8$  T with varying temperature from 10 to 300 K; (c) at  $T = 300$  K; and (d)  $T = 10$  K with varying magnetic fields from 0 to 8 T.

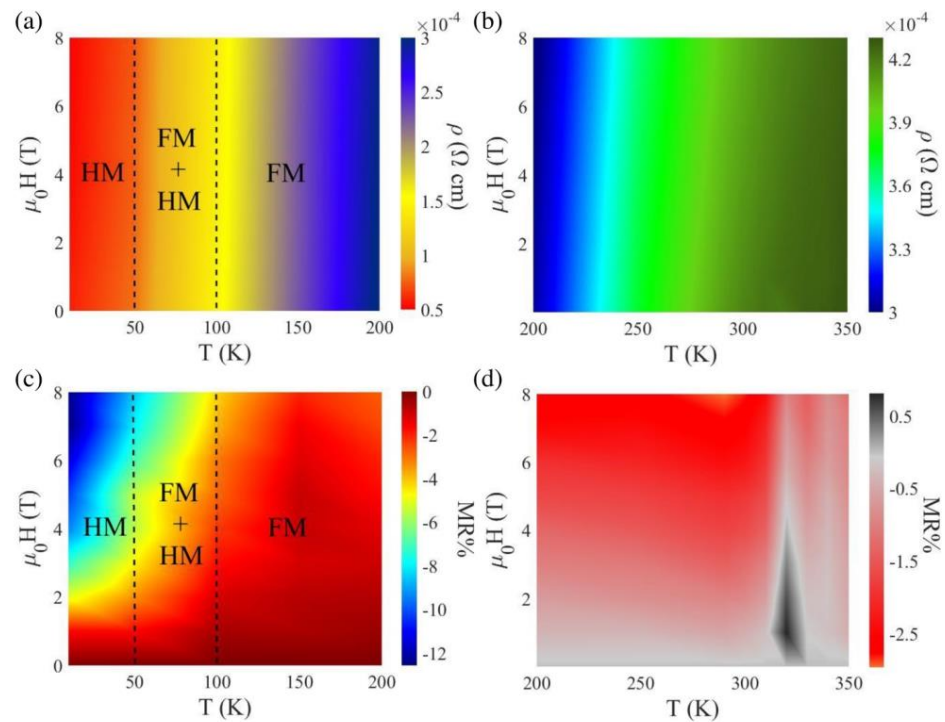


**Figure 5.** Magnetic field and temperature dependent 2D-surface plots of (a) resistivity and (c) magnetoresistance in the temperature range  $2\text{ K} < T < 200\text{ K}$  and (b) resistivity and (d) magnetoresistance in the temperature range  $200\text{ K} < T < 350\text{ K}$ .

#### 4. Conclusions

In conclusion, the temperature and magnetic field-dependent charge transport properties of the MnP nanorod thin film have been studied systematically. The MnP film exhibits a metallic behavior over the entire measured temperature range (5–350 K). The intrinsic electrical resistivity of the MnP film displays the  $T^2$  dependence at low temperatures (<50 K) and a linear dependence at higher temperatures. A large negative magnetoresistance of up to 12% is observed in the helical magnetic regime ( $T < \sim 50$  K), under the application of high magnetic fields up to 8 T. The magnetic transitions from the PM to FM phase and from the FM to stable HM phase, as well as the field-driven conversion of magnetic phases (e.g., CONE, FAN) are also revealed from the magneto-transport data. It has been established that the low temperature magnetoresistance is dominated by the intergranular spin-dependent tunneling mechanism. Our study pinpoints the correlation between the transport and magnetism in this helimagnetic system.

**Author Contributions:** Conceptualization, B.M. and M.-H.P.; resource, A.T.D.; investigation, B.M., M.-T.T., R.P.M., D.D., C.-M.H., N.W.Y.A.Y.M. and A.C.; data curation, B.M. and A.C.; writing—original draft preparation, B.M.; writing—review and editing, R.P.M., M.-T.T., A.C., S.W. and M.-H.P.; supervision, M.-H.P.; project administration, M.-H.P.; funding acquisition, M.-H.P. All authors have read and agreed to the published version of the manuscript.

**Funding:** This research was funded by the US Department of Energy, Office of Basic Energy Sciences, Division of Materials Science and Engineering under Grant No. DE-FG02-07ER46438.

**Data Availability Statement:** The data presented in this study are available on request from the corresponding author.

**Acknowledgments:** The authors thank Sunglae Cho of the University of Ulsan and Pham Thanh Huy of Phenikaa University for their useful discussions.

**Conflicts of Interest:** The authors declare no conflict of interest.

#### References

1. Felcher, G.P. Magnetic Structure of MnP. *J. Appl. Phys.* **2004**, *37*, 1056. [[CrossRef](#)]
2. Obara, H.; Endoh, Y.; Ishikawa, Y.; Komatsubara, T. Magnetic Phase Transition of MnP under Magnetic Field. *J. Phys. Soc. Jpn.* **1980**, *49*, 928–935. [[CrossRef](#)]
3. Matsuda, M.; Ye, F.; Dissanayake, S.E.; Cheng, J.-G.; Chi, S.; Ma, J.; Zhou, H.D.; Yan, J.-Q.; Kasamatsu, S.; Sugino, O.; et al. Uwatoko, Pressure dependence of the magnetic ground states in MnP. *Phys. Rev. B* **2016**, *93*, 100405. [[CrossRef](#)]
4. Huber, E.E.; Ridgley, D.H. Magnetic properties of a single crystal of manganese phosphide. *Phys. Rev.* **1964**, *135*, A1033. [[CrossRef](#)]
5. Suzuki, T. Magnetic field effects on the thermoelectric power in MnP single crystal. *J. Phys. Soc. Jpn.* **1969**, *26*, 279–283. [[CrossRef](#)]
6. Reis, M.S.; Rubinger, R.M.; Sobolev, N.A.; Valente, M.A.; Yamada, K.; Sato, K.; Todate, Y.; Bouravleuv, A.; Von Ranke, P.J.; Gama, S. Influence of the strong magnetocrystalline anisotropy on the magnetocaloric properties of MnP single crystal. *Phys. Rev. B* **2008**, *77*, 104439. [[CrossRef](#)]
7. Booth, R.A.; Majetich, S.A. Crystallographic orientation and the magnetocaloric effect in MnP. *J. Appl. Phys.* **2009**, *105*, 7–926. [[CrossRef](#)]
8. Monette, G.; Nateghi, N.; Masut, R.A.; Francoeur, S.; Ménard, D. Plasmonic enhancement of the magneto-optical response of MnP nanoclusters embedded in GaP epilayers. *Phys. Rev. B* **2012**, *86*, 245312. [[CrossRef](#)]
9. Chong, X.Y.; Jiang, Y.H.; Zhou, R.; Feng, J. Pressure dependence of electronic structure and superconductivity of the MnX (X = N, P, As, Sb). *Sci. Rep.* **2016**, *6*. [[CrossRef](#)]
10. Wang, Y.; Feng, Y.; Cheng, J.G.; Wu, W.; Luo, J.L.; Rosenbaum, T.F. Spiral magnetic order and pressure-induced superconductivity in transition metal compounds. *Nat. Commun.* **2016**, *7*, 13037. [[CrossRef](#)]
11. Cheng, J.-G.; Matsubayashi, K.; Wu, W.; Sun, J.P.; Lin, F.K.; Luo, J.L.; Uwatoko, Y. Pressure Induced Superconductivity on the border of Magnetic Order in MnP. *Phys. Rev. Lett.* **2015**, *114*, 117001. [[CrossRef](#)] [[PubMed](#)]
12. Luo, J.; Cheng, J.; Qin, Y.; Shen, Y. Pressure-induced superconductivity in CrAs and MnP. *J. Phys. Condens. Matter.* **2017**, *29*, 383003. [[CrossRef](#)] [[PubMed](#)]
13. Shiomi, Y.; Iguchi, S.; Tokura, Y. Emergence of topological Hall effect from fanlike spin structure as modified by Dzyaloshinsky-Moriya interaction in MnP. *Phys. Rev. B* **2012**, *86*, 180404. [[CrossRef](#)]
14. Ohbayashi, M.; Komatsubara, T.; Hirahara, E. De Haas-Van Alphen Effect in Manganese Phosphide. *J. Phys. Soc. Jpn.* **1976**, *40*, 1088–1094. [[CrossRef](#)]

15. Kawakatsu, S.; Kakihana, M.; Nakashima, M.; Amako, Y.; Nakamura, A.; Aoki, D.; Takeuchi, T.; Harima, H.; Hedou, M.; Nakama, T.; et al. De Haas–Van Alphen experiment and Fermi surface properties in field-induced ferromagnetic state of MnP. *J. Phys. Soc. Jpn.* **2019**, *88*, 044705. [[CrossRef](#)]
16. Takase, A.; Kasuya, T. High field magnetoresistance in MnP. *J. Phys. Soc. Jpn.* **1980**, *49*, 489–492. [[CrossRef](#)]
17. Jiang, N.; Nii, Y.; Arisawa, H.; Saitoh, E.; Onose, Y. Electric current control of spin helicity in an itinerant helimagnet. *Nat. Commun.* **2020**, *11*, 1601. [[CrossRef](#)]
18. Matsumura, Y.; Narita, E.; Hirahara, E. Effect of Uniaxial Pressure on the Magnetic Transition Temperatures in Manganese Phosphide. *J. Phys. Soc. Jpn.* **1975**, *38*, 1264–1269. [[CrossRef](#)]
19. Duong, A.T.; Nguyen, T.M.H.; Nguyen, D.L.; Das, R.; Nguyen, H.T.; Phan, B.T.; Cho, S. Enhanced magneto-transport and thermoelectric properties of MnP nanorod thin films grown on Si (1 0 0). *J. Magn. Magn. Mater.* **2019**, *482*, 287–291. [[CrossRef](#)]
20. Pokharel Madhogaria, R.; Hung, C.-M.; Muchharla, B.; Tuan Duong, A.; Das, R.; Thanh Huy, P.; Cho, S.; Witanachchi, S.; Srikanth, H.; Phan, M.-H. Strain-modulated helimagnetism and emergent magnetic phase diagrams in highly crystalline MnP nanorod films. *Phys. Rev. B* **2021**, *103*, 184423. [[CrossRef](#)]
21. Zheng, P.; Xu, Y.J.; Wu, W.; Xu, G.; Lv, J.L.; Lin, F.K.; Wang, P.; Yang, Y.F.; Luo, J.L. Orbital-dependent charge dynamics in MnP revealed by optical study. *Sci. Rep.* **2017**, *7*, 14178. [[CrossRef](#)] [[PubMed](#)]
22. Sun, X.; Zhao, S.; Bachmatiuk, A.; Rümmele, M.H.; Gorantla, S.; Zeng, M.; Fu, L. 2D Intrinsic Ferromagnetic MnP Single Crystals. *Small* **2020**, *16*, e2001484. [[CrossRef](#)] [[PubMed](#)]
23. De Andrés, A.; Espinosa, A.; Prieto, C.; Garca-Hernández, M.; Ramirez-Jiménez, R.; Lambert-Milot, S.; Masut, R.A. MnP films and MnP nanocrystals embedded in GaP epilayers grown on GaP(001): Magnetic properties and local bonding structure. *J. Appl. Phys.* **2011**, *109*, 113910. [[CrossRef](#)]
24. Venkateswarlu, B.; Midhunlal, P.V.; Babu, P.D.; Kumar, N.H. Magnetic and anomalous electronic transport properties of the quaternary Heusler alloys Co<sub>2</sub>Ti<sub>1-x</sub>FexGe. *J. Magn. Magn. Mater.* **2016**, *407*, 142–147. [[CrossRef](#)]
25. Urushibara, A.; Moritomo, Y.; Arima, T.; Asamitsu, A.; Kido, G.; Tokura, Y. Insulator-Metal Transition and Giant Magnetoresistance in La<sub>1-x</sub>Sr<sub>x</sub>MnO<sub>3</sub>. *Phys. Rev. B* **1995**, *51*, 14103. [[CrossRef](#)]
26. Kubo, K.; Ohatata, N. A Quantum Theory of Double Exchange. *I. J. Phys. Soc. Jpn.* **1972**, *33*, 21–32. [[CrossRef](#)]
27. Chatterjee, S.; Chatterjee, S.; Giri, S.; Majumdar, S. Transport Properties of Heusler Compounds and Alloys. *J. Phys. Condens. Matter.* **2021**, *34*, 013001. [[CrossRef](#)]
28. Kim, D.; Li, Q.; Syers, P.; Butch, N.P.; Paglione, J.; Sarma, S.D.; Fuhrer, M.S. Intrinsic electron-phonon resistivity of Bi<sub>2</sub>Se<sub>3</sub> in the topological regime. *Phys. Rev. Lett.* **2012**, *109*, 166801. [[CrossRef](#)]
29. Sankar, S.; Berkowitz, A.E.; Smith, D.J. Spin-dependent transport of Co-SiO<sub>2</sub> granular films approaching percolation. *Phys. Rev. B* **2000**, *62*, 14273. [[CrossRef](#)]
30. Wu, J.; Lynn, J.W.; Glinka, C.J.; Burley, J.; Zheng, H.; Mitchell, J.F.; Leighton, C. Intergranular Giant Magnetoresistance in a Spontaneously Phase Separated Perovskite Oxide. *Phys. Rev. Lett.* **2005**, *94*, 037201. [[CrossRef](#)]
31. Inoue, J.; Maekawa, S. Theory of tunneling magnetoresistance in granular magnetic films. *Phys. Rev. B* **1996**, *53*, R11927. [[CrossRef](#)] [[PubMed](#)]

**Disclaimer/Publisher’s Note:** The statements, opinions and data contained in all publications are solely those of the individual author(s) and contributor(s) and not of MDPI and/or the editor(s). MDPI and/or the editor(s) disclaim responsibility for any injury to people or property resulting from any ideas, methods, instructions or products referred to in the content.